Supporting Information: Influence of molecular weight on ion-transport properties of polymeric ionic liquids

Jordan R. Keith[1], Santosh Mogurampelly[1], Faisal Aldukhi[1,2], Bill K. Wheatle[1], and Venkat Ganesan[1]

[1]*Department of Chemical Engineering, The University of Texas at Austin, Austin, TX USA*

[2]*Department of Chemical and Biomolecular Engineering, University of Illinois at Urbana-Champaign, Champaign, IL USA*

Email: venkat@che.utexas.edu

Phone: 512-471-4856

Abstract

In this supporting information we provide details related to the article "Influence of the number of repeat units on ion-transport properties of polymeric ionic liquids." Herein, we document the force field parameters used to run molecular dynamics simulations of an all-atom representation of 1-butyl-3-vinylimidazolium-hexafluorophosphate ionic liquids. This includes Lennard-Jones parameters and partial atomic charges for non-bonded interactions, along with bond, angle, dihedral, and improper parameters for intramolecular interactions. Mean-squared displacement and ion-pair autocorrelation curves are presented to supplement the diffusivities and ion-pair relaxation times presented in the main article. The method of identifying diffusivity from collections of similar coordination properties is expanded upon from what was presented in the main article. We make a few comments on the glass transition temperature on the compounds studied in this report. Through this presentation, we defend our choice to use interpolated temperatures from experimental glass transition temperatures of the pure ionic liquid and an infinite chain polymer, as opposed to temperatures extracted from simulation. We present energy and density profiles over the length of the simulations to confirm that the systems within are equilibrated and are running at steady state. Finally, we present a short discussion on the density, and its possible impacts on the quantities explored in this report.

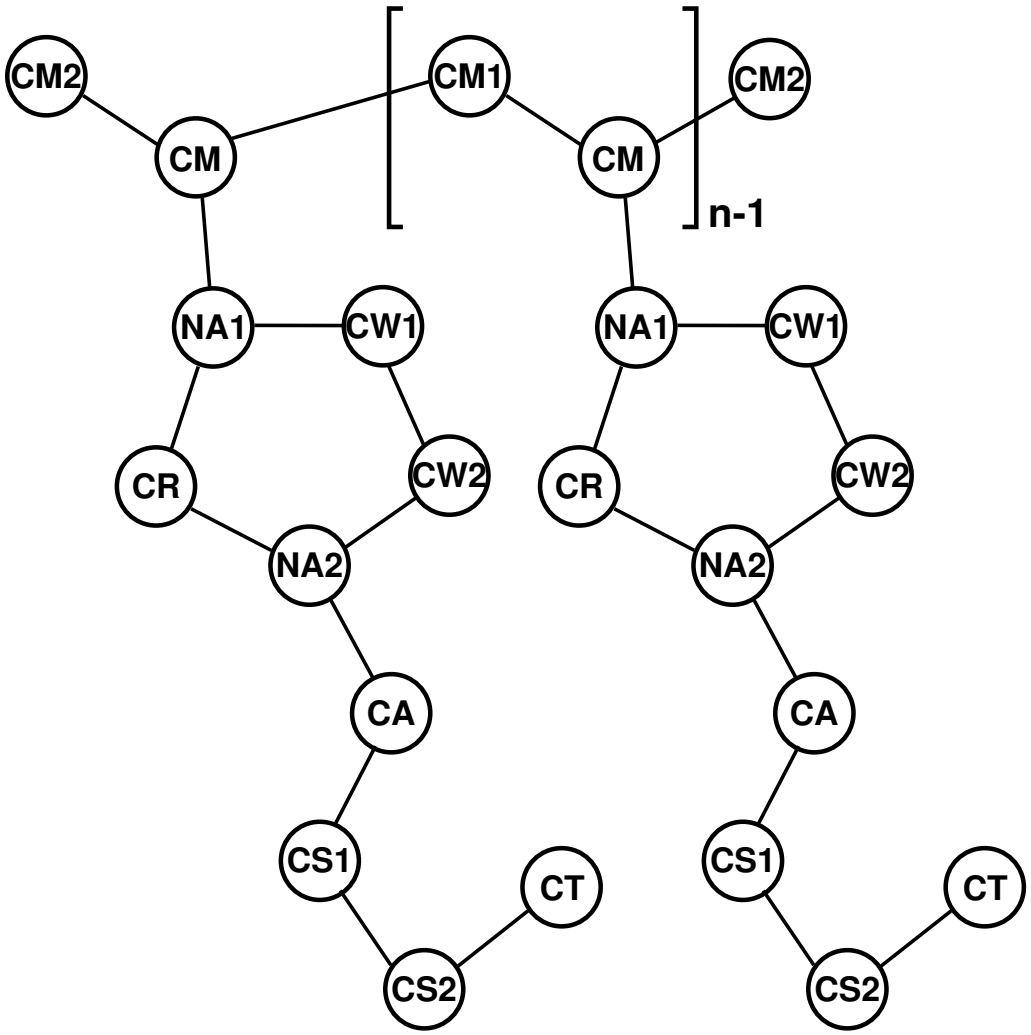

FIG. S1. Representation of the atoms contained in the polymer under investigation (poly(1-butyl-3-vinylimdazolium), with names matching those employed in defining the force field parameters in Tables S1-S7. The PF_6^- atoms (OP, PF1, PF2, and PF3) are excluded to ensure clariity of the polymeric atoms.

I. METHODS

A. Force Field Parameters

This section reports Lennard-Jones parameters and partial charges (Table S1); as well as bond (Table S2), angle (Tables S3 and S4), and dihedral (Table S5 and S6) parameters, as used in the force field described in the main article. The potential equations are presented

#	Atom Type	ϵ_{lj} (kcal/mol)	σ_{lj} (Å)	q (e)
1	CA[1–3]	0.0660	3.5000	-0.071916
2	CM[1–3]	0.0660	3.5000	-0.191281
3	CM1[1–3]	0.0660	3.5000	-0.286559
4	CM2[1–3]	0.0660	3.5000	-0.286559
5	CR[1–3]	0.0700	3.5500	-0.081640
6	CS1[1–3]	0.0660	3.5000	-0.112314
7	CS2[1–3]	0.0660	3.5000	0.058799
8	CT[1–3]	0.0660	3.5000	-0.168031
9	CW1[1–3]	0.0700	3.5500	-0.203382
10	CW2[1–3]	0.0700	3.5500	-0.165764
11	HA[1,4]	0.0300	1.9200	0.103288
12	HM[1,4]	0.0300	1.9200	0.200553
13	HM1[1–3]	0.0300	2.5000	0.198717
14	HM2[1–3]	0.0300	2.5000	0.132478
15	HM3[1–3]	0.0300	2.5000	0.0955197
16	HR[1,4]	0.0300	1.9200	0.215218
17	HS1[1–3]	0.0300	2.5000	0.063370
18	HS2[1–3]	0.0300	2.5000	0.032434
19	HT[1–3]	0.0300	2.5000	0.056042
20	HW1[1,4]	0.0300	1.7200	0.238040
21	HW2[1,4]	0.0300	1.7200	0.244756
22	NA1[1–3]	0.1700	3.2500	0.276722
23	NA2[1–3]	0.1700	3.2500	0.083055
24	*OP[1,4]	0.2000	3.9400	1.340000
25	*PF1[1–3]	0.0610	3.1181	-0.390000
26	*PF2[1–3]	0.0610	3.1181	-0.390000
27	*PF3[1–3]	0.0610	3.1181	-0.390000

TABLE S1. **Lennard-Jones parameters and unscaled partial charges**, *Partial charges used from listed source

in detail in section II.A of the main paper. Information related to the development of the force field parameters are presented in section II.B. of the main paper. Missing details on development of the backbone carbon and hydrogen parameters can be found in Reference 1. Figure S1 depicts the atoms as they exist within the polymer. The PF_6^- atoms are excluded from this drawing. The phosphorous (OP) atom is central, and is surrounded by six fluorine atoms (2 PF1, 2 PF2, and 2 PF3). Unlike fluorine atoms are positioned at 90 degree angles, while like fluorine atoms are positioned at 180 degree angles. This is clear in Table S4.

#	Bond Type	k_r (kcal/mol-Å^2)	r_0 (Å)
1	CA-CS1[1]	280.159	1.534
2	CA-HA[1]	357.723	1.092
3	CA-NA2[1]	287.313	1.478
4	CM-CM1[1]	276.101	1.532
5	CM-CM2[1]	276.101	1.532
6	CM-HM[1]	363.651	1.083
7	CM-NA1[1]	274.189	1.486
8	CM1-HM1[1]	348.875	1.095
9	CM2-HM2[1]	348.875	1.095
10	CM2-HM3[1]	348.875	1.095
11	CR-HR[1]	401.204	1.074
12	CR-NA1[1]	464.417	1.385
13	CR-NA2[1]	552.388	1.335
14	CS1-CS2[1]	281.515	1.536
15	CS1-HS1[1]	347.494	1.091
16	CS2-CT[1]	287.616	1.532
17	CS2-HS2[1]	349.100	1.095
18	CT-HT[1]	351.780	1.093
19	CW1-CW2[1]	531.524	1.352
20	CW1-HW1[1]	396.395	1.081
21	CW1-NA1[1]	410.333	1.386
22	CW2-HW2[1]	395.457	1.079
23	CW2-NA2[1]	408.436	1.384
24	OP-PF1[1–3]	500.000	1.596
25	OP-PF2[1–3]	500.000	1.596
26	OP-PF3[1–3]	500.000	1.596

TABLE S2. **Harmonic bond parameters**

II. ANALYZING RESULTS FOR ACCURACY AND CONSISTENCY

A. Mean-squared displacement and extracting diffusivity

When computing diffusivity from a simulation of finite time, a good approximation of the true diffusivity can be found by fitting a representative time range to a power-law fit,

$$\left\langle \big(\mathbf{r}(t) - \mathbf{r}(0)\big)^2 \right\rangle = C_0 \tau^{\beta} + C_1, \tag{S1}$$

#	Cent Atom	Outer Atoms	k_θ (kcal/mol-rad^2)	θ_0 (deg)
1	CA	CS1-HA[1]	63.034	111.966
2	CA	CS1-NA2[1]	78.829	112.124
3	CA	HA-HA[1]	63.013	107.853
4	CA	HA-NA2[1]	71.809	106.307
5	CM	CM1-CM1[1]	86.605	113.354
6	CM	CM1-CM2[1]	86.605	113.354
7	CM	CM1-HM[1]	62.360	109.018
8	CM	CM1-NA1[1]	100.742	109.948
9	CM	CM2-HM[1]	62.360	109.018
10	CM	CM2-NA1[1]	100.742	109.948
11	CM1	CM-CM[1]	93.377	116.755
12	CM1	CM-HM1[1]	65.863	109.352
13	CM1	HM1-HM1[1]	54.233	108.068
14	CM2	CM-HM2[1]	65.863	109.352
15	CM2	CM-HM3[1]	65.863	109.352
16	CM2	HM2-HM2[1]	54.233	108.068
17	CM2	HM3-HM3[1]	54.233	108.068
18	CR	HR-NA1[1]	64.617	125.669
19	CR	HR-NA2[1]	66.082	125.132
20	CR	NA1-NA2[1]	252.744	109.164
21	CS1	CA-CS2[1]	80.939	112.443
22	CS1	CA-HS1[1]	67.208	109.146
23	CS1	CS2-HS1[1]	55.219	108.941
24	CS1	HS1-HS1[1]	56.563	107.458
25	CS2	CS1-CT[1]	80.400	114.212
26	CS2	CS1-HS2[1]	59.461	107.908
27	CS2	CT-HS2[1]	58.884	109.477
28	CS2	HS2-HS2[1]	82.095	106.005
29	CT	CS2-HT[1]	63.976	111.352
30	CT	HT-HT[1]	68.335	108.358
31	CW1	CW2-HW1[1]	58.627	130.162
32	CW1	CW2-NA1[1]	255.171	106.709
33	CW1	HW1-NA1[1]	68.306	122.790
34	CW2	CW1-HW2[1]	64.721	130.027
35	CW2	CW1-NA2[1]	268.303	107.291
36	CW2	HW2-NA2[1]	61.818	122.991
37	NA1	CM-CR[1]	90.685	126.384
38	NA1	CM-CW1[1]	97.374	125.886
39	NA1	CR-CW1[1]	266.725	107.813
40	NA2	CA-CR[1]	84.594	126.178

TABLE S3. **Harmonic angle parameters**, *[CM1-NA1 (11), CM1-NA1 (12), CM1-NA1 (13), CM2-NA1 (15), CM2-NA1 (16), CM2-NA1 (17)][1]

#	Cent Atom	Outer Atoms	k_θ (kcal/mol-rad^2)	θ_0 (deg)
41	NA2	CA-CW2[1]	88.387	126.334
42	NA2	CR-CW2[1]	97.245	108.165
43	OP	PF1-PF1[2,3]	75.000	180.000
44	OP	PF1-PF2[2,3]	75.000	90.000
45	OP	PF1-PF3[2,3]	75.000	90.000
46	OP	PF2-PF2[2,3]	75.000	180.000
47	OP	PF2-PF3[2,3]	75.000	90.000
48	OP	PF3-PF3[2,3]	75.000	180.000

TABLE S4. **Harmonic angle parameters (cont.)**

and if the parameter β is close to unity, then the apparent diffusivity is calculated from

$$D_{apparent} = \frac{1}{6} C_0. \tag{S2}$$

Our choice for this representative time range was 20 ns to 35 ns, and the validity of this choice is supported by the results in Table S7 and Figure S2. Stated differently, only τ-values between 20 ns and 35 ns were used to develop a least-square fit of each MSD to Equation S1. Table S7 shows values of the linearity exponent β for all systems and temperatures. Many of these values are within 10% of unity, and almost all of the values fall within 20%. We showed in a previous report that the diffusivity undergoes negligible changes from such a representation, even when β approaches one over much longer simulations.[1] Figure S2 shows the mean-squared displacement (MSD) curves with respect to time. This should give the reader a visual representation of the curves used to fit diffusivity, along with some visual interpretation of the linearity β of the long-time regions for the different systems. Error bars are displayed on diffusivity in figures throughout the main article. These errors represent 95% confidence intervals for a set of diffusivties obtained from each MSD curve over separate 10 ns intervals, assuming that such a dataset can be represented by a normal distribution. This means that each curve supplied between five and seven different values for diffusivity (50-70 ns simulation lengths). However, it would be best to represent such error by computing diffusivities on MSDs from different system configurations, but we refrained from using this approach due to the vast amount of additional computing resources required to achieve this objective.

#	Cent Bond	Outer Atoms	K_1 (kcal/mol)	K_2 (kcal/mol)	K_3 (kcal/mol)	K_4 (kcal/mol)
1	CA-CS1	CS2-HA[2,3]	0.000	0.000	0.366	0.000
2	CA-CS1	CS2-NA2[2,3]	-1.788	0.756	-0.288	0.000
3	CA-CS1	HA-HS1[2,3]	0.000	0.000	0.318	0.000
4	CA-CS1	HS1-NA2[2,3]	0.000	0.000	0.000	0.000
5	CA-NA2	CR-CS1[2,3]	-1.659	-0.555	-0.375	0.000
6	CA-NA2	CR-HA[2,3]	0.000	0.000	0.000	0.000
7	CA-NA2	CS1-CW2[2,3]	-1.910	-1.500	0.290	0.000
8	CA-NA2	CW2-HA[2,3]	-1.400	-2.650	0.175	0.000
9	CM-CM1	CM-CM1[1]	-0.775803	0.313249	4.69238	0.31007
10	CM-CM1	CM-CM2[1]	-0.775803	0.313249	4.69238	0.31007
11	CM-CM1	CM-HM[1]	0.000	0.000	2.677	0.000
12	CM-CM1	CM1-HM1[1]	0.000	0.000	2.677	0.000
13	CM-CM1	CM2-HM1[1]	0.000	0.000	2.677	0.000
14	CM-CM1	HM-HM1[1]	0.000	0.000	2.78174	0.000
15	CM-CM1	CM-NA1[1]	0.000	0.000	4.44212	0.000
16	CM-CM1	HM1-NA1[1]	-0.839253	-0.310509	4.68038	0.846371
17	CM-CM2	CM1-HM2[1]	0.000	0.000	2.677	0.000
18	CM-CM2	CM1-HM3[1]	0.000	0.000	2.677	0.000
19	CM-CM2	HM-HM2[1]	0.000	0.000	2.78174	0.000
20	CM-CM2	HM-HM3[1]	0.000	0.000	2.78174	0.000
21	CM-CM2	HM2-NA1[1]	-0.839253	-0.310509	4.68038	0.846371
22	CM-CM2	HM3-NA1[1]	-0.839253	-0.310509	4.68038	0.846371
23	CM-NA1	CM1-CR[1]	2.45324	-0.559275	-0.813571	1.52831
24	CM-NA1	CM2-CR[1]	2.45324	-0.559275	-0.813571	1.52831
25	CM-NA1	CR-HM[1]	0.000	0.000	0.000	0.000
26	CM-NA1	CM1-CW1[1]	0.000	0.000	2.37904	0.000
27	CM-NA1	CM2-CW1[1]	0.000	0.000	2.37904	0.000
28	CM-NA1	CW1-HM[1]	0.000	0.000	0.124	0.000
29	CR-NA1	CM-HR[1]	0.000	4.651	0.000	0.000
30	CR-NA1	CM-NA2[1]	0.000	4.651	0.000	0.000
31	CR-NA1	CW1-HR[2,3]	0.000	4.651	0.000	0.000
32	CR-NA1	CW1-NA2[2,3]	0.000	4.651	0.000	0.000
33	CR-NA2	CA-HR[2,3]	0.000	4.651	0.000	0.000
34	CR-NA2	CA-NA1[2,3]	0.000	4.651	0.000	0.000
35	CR-NA2	CW2-HR[2,3]	0.000	4.651	0.000	0.000
36	CR-NA2	CW2-NA1[2,3]	0.000	4.651	0.000	0.000
37	CS1-CS2	CA-CT[2,3]	1.300	-0.050	0.200	0.000
38	CS1-CS2	CA-HS2[2,3]	0.000	0.000	0.366	0.000
39	CS1-CS2	CT-HS1[2,3]	0.000	0.000	0.366	0.000
40	CS1-CS2	HS1-HS2[2,3]	0.000	0.000	0.318	0.000

TABLE S5. **OPLS dihedral parameters**

#	Cent Bond	Outer Atoms	K_1 (kcal/mol)	K_2 (kcal/mol)	K_3 (kcal/mol)	K_4 (kcal/mol)
41	CS2-CT	CS1-HT[2,3]	0.000	0.000	0.366	0.000
42	CS2-CT	HS2-HT[2,3]	0.000	0.000	0.318	0.000
43	CW1-CW2	HW1-HW2[2,3]	0.000	10.75	0.000	0.000
44	CW1-CW2	HW1-NA2[2,3]	0.000	10.75	0.000	0.000
45	CW1-CW2	HW2-NA1[2,3]	0.000	10.75	0.000	0.000
46	CW1-CW2	NA1-NA2[2,3]	0.000	10.75	0.000	0.000
47	CW1-NA1	CM-CW2[1]	0.000	3.000	0.000	0.000
48	CW1-NA1	CM-HW1[1]	0.000	3.000	0.000	0.000
49	CW1-NA1	CR-CW2[2,3]	0.000	3.000	0.000	0.000
50	CW1-NA1	CR-HW1[2,3]	0.000	3.000	0.000	0.000
51	CW2-NA2	CA-CW1[2,3]	0.000	3.000	0.000	0.000
52	CW2-NA2	CA-HW2[2,3]	0.000	3.000	0.000	0.000
53	CW2-NA2	CR-CW1[2,3]	0.000	3.000	0.000	0.000
54	CW2-NA2	CR-HW2[2,3]	0.000	3.000	0.000	0.000

TABLE S6. **OPLS dihedral parameters (cont.)**

n	β (500 K)	β (525 K)	β (550 K)	β (575 K)	β (600 K)
2	1.03200	0.9955	0.95799	1.0155	1.01590
3	0.94486	0.96033	0.9679	1.0108	1.02210
5	0.91536	0.82791	0.8711	0.91215	0.96327
7	0.84129	0.81313	—	0.8815	0.94215
8	0.79342	0.91158	0.81713	0.93951	0.92530
9	0.89820	0.83218	0.84141	0.93819	0.93566
10	0.77736	0.87668	—	0.97772	0.95535
11	0.86832	0.90548	0.91904	0.91901	0.96215
12	0.88318	0.90548	0.91904	0.91901	0.89316
16	0.85417	0.81435	0.80025	0.84655	0.89824

TABLE S7. β linearity parameter (MSD $\sim t^{\beta}$) for all systems studied in this work

Using the data of our previous work for $n = 32$,[1] we tested the validity of diffusivity values from "short" timescales (30 ns) versus those from "long" timescales (300 ns). The data is displayed in Figure S3, and demonstrates that simulating this system for an additoonal order of magnitude does not appreciably change the diffusion coefficient. Table S8 shows β linearity parameters for the cases examined in this figure. It can be seen that, at and above 500 K, the "short" timescale maintains a high degree of linearity (within 20% of $\beta = 1$). We are, therefore, confident in the validity of the data from the present work due to the following considerations: 1) temperatures of 500 K and higher, 2) shorter polyILs (faster relaxation),

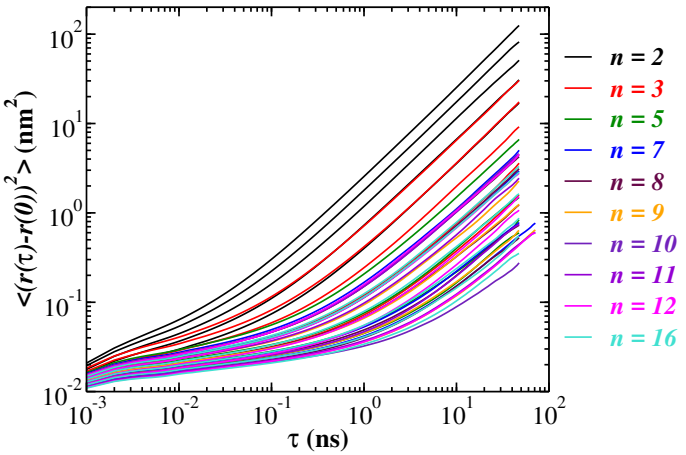

FIG. S2. Mean-squared displacement for all systems analyzed in this study, plotted on logarithmic axes for clarity of low-displacement curves and identification of curvature for β linearity exponent

$T(K)$	β_{30ns}	β_{300ns}
350	0.44	0.84
375	0.37	0.88
400	0.57	0.92
425	0.62	0.91
450	0.70	0.92
475	0.74	0.86
500	0.83	0.91
525	0.85	0.91
550	0.91	0.90
575	0.86	0.94
600	0.91	0.95

TABLE S8. β linearity parameter for data shown in Figure S3

and 3) trajectories analyzed over a minimum of 50 ns.

B. Quantifying diffusivity of ions binned by coordination state

We present results in the main article detailing differences in diffusion coefficient across subsets of PF_6^- ions experiencing varying degrees of coordination. Specifically, we investigate differences among various ranges of ionic (N_c), inter-polymeric (N_p), and intra-polymeric (N_{cp}) values. These ranges are unique to the different systems, and the values for the upper and lower bounds of each subset (eight subsets total) can be found in Tables S9 ($n = 5$), S10

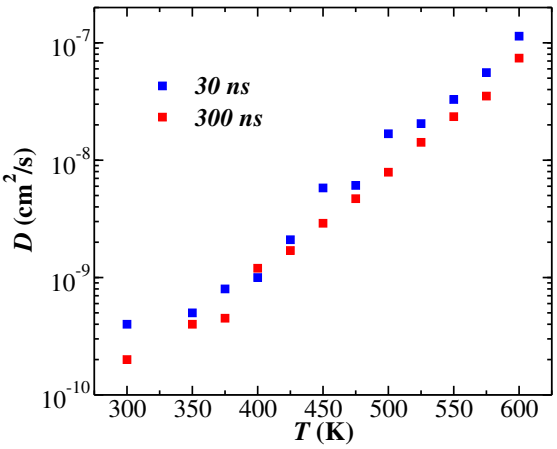

FIG. S3. Diffusion coefficient for $n = 32$ calculated from short and long trajectories. The changes in D are marginal and the qualitative features have been preserved with a longer trajectory. Data taken from Reference 1 with permission from ACS.

($n = 8$), S11, and S12 ($n = 16$). The number of PF_6^- ions counted in each subset is also reported in these previous tables, to give the reader an idea of the prevalence (and quality of the underlying statistics) for each diffusivity result presented in Figure 9 of the main article. Furthermore, Figures S4 ($n = 5$), S5 ($n = 8$), S6 ($n = 12$), and S7 ($n = 16$) present the actual mean-squared displacement curves for each subset of each system. We utilized the previously described procedure, fitting data over the same time range (20-35 ns) used on the full trajectory, for extracting diffusivities over these binned datasets. Although some of the curves appear to be quite poor for the purpose of collecting a diffusivity, most of the resulting curves are appropriate for fitting a diffusivity for the purposes described in the main article. By containing analysis from these curves within this comparison among other binned results, we ensure that any error caused by the small sample sizes or non-linearity of mean-squared displacement curves does not filter outside of the present analysis.

C. Ion-pair autocorrelation functions

Figure S8 presents the plot of the autocorrelation functions $C(\tau)$ and $S(\tau)$ as a function of time τ. This is meant to give the reader a visual understanding of the decay of ion pairs across the simulation for polyIL systems at various temperatures. Figure 8(a) shows the decay of

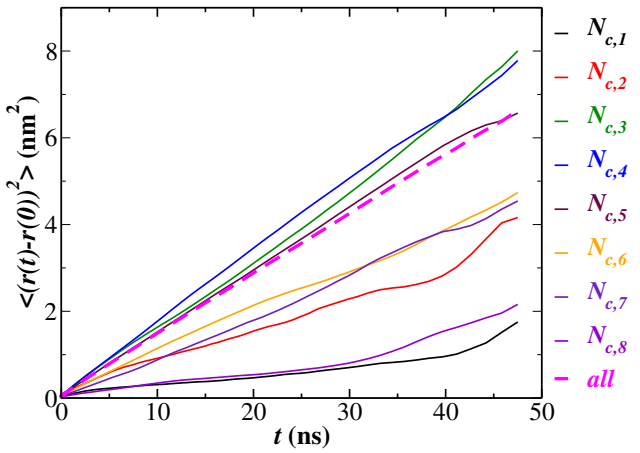

(a)

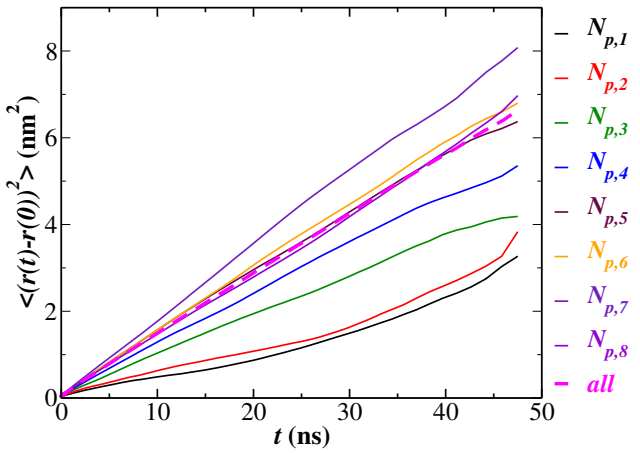

(b)

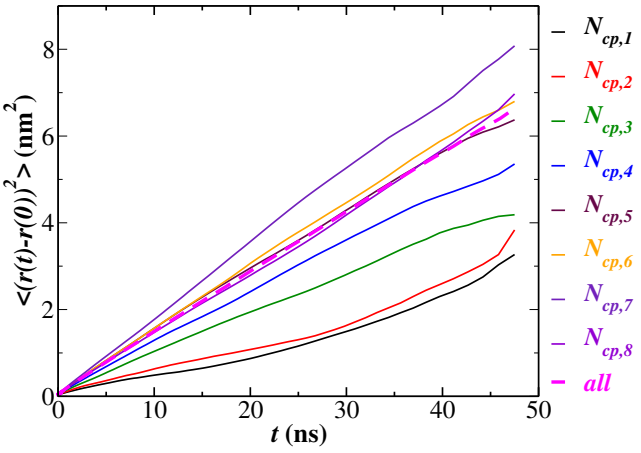

(c)

FIG. S4. MSD for subsets of $n = 5$ polyIL, sorted by (a) average N_c and (b) average N_p and (c) average N_{cp}.

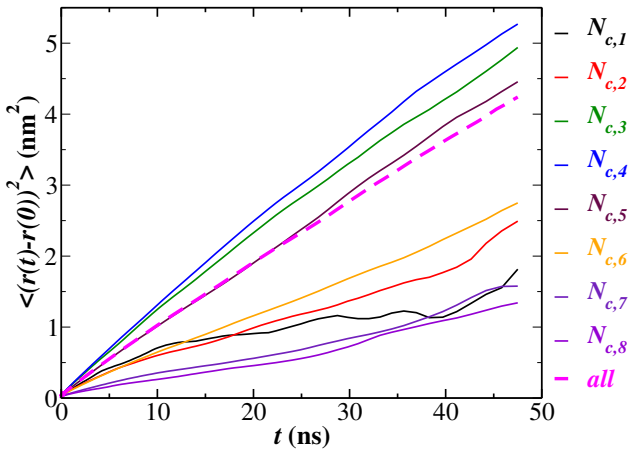

(a)

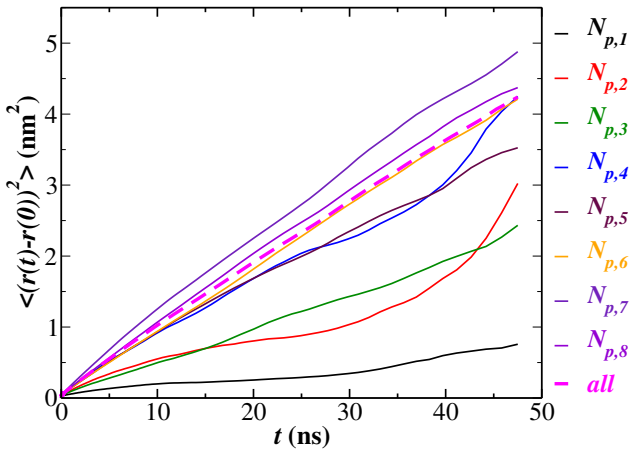

(b)

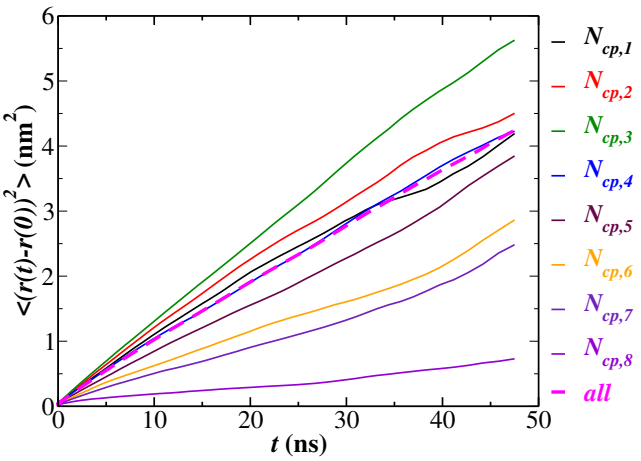

(c)

FIG. S5. MSD for subsets of $n = 8$ polyIL, sorted by (a) average N_c and (b) average N_p and (c) average N_{cp}.

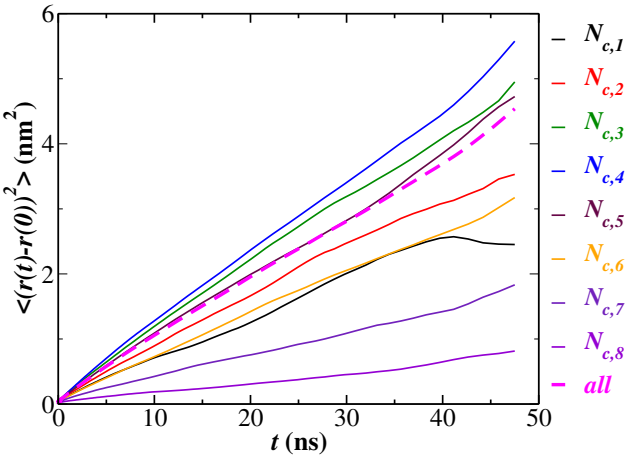

(a)

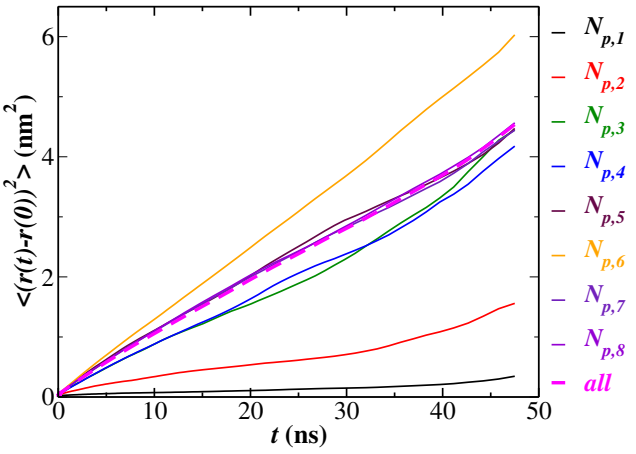

(b)

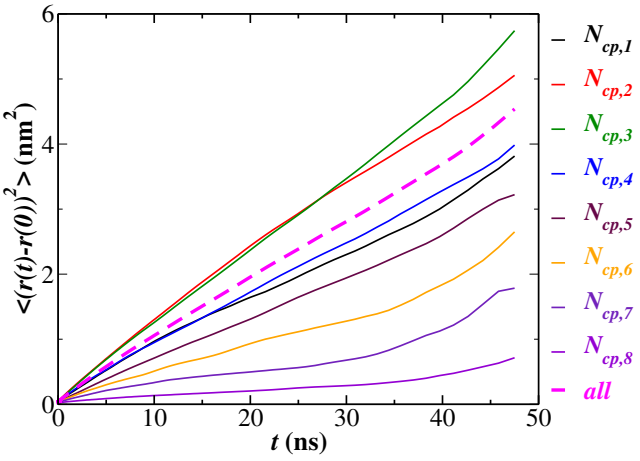

(c)

FIG. S6. MSD for subsets of $n = 12$ polyIL, sorted by (a) average N_c and (b) average N_p and (c) average N_{cp}.

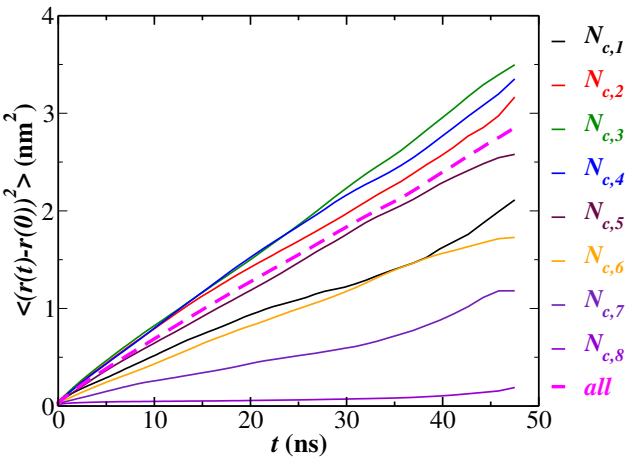

(a)

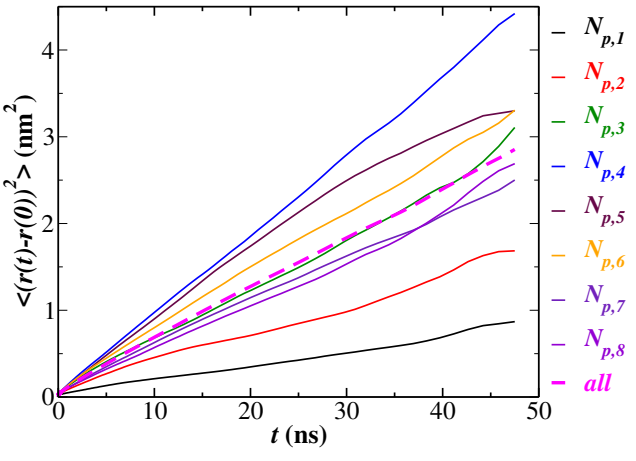

(b)

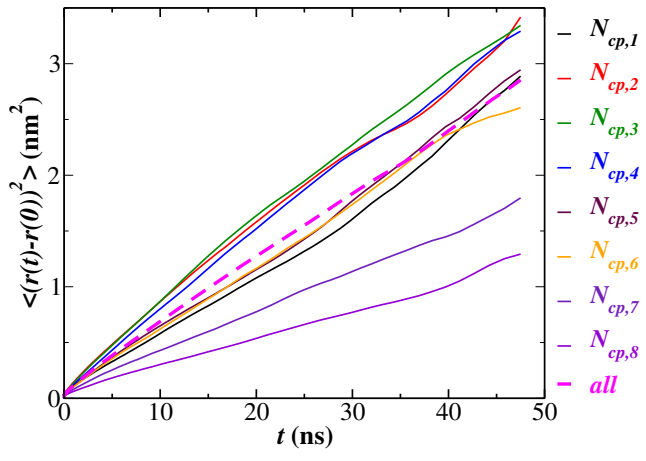

(c)

FIG. S7. MSD for subsets of $n = 16$ polyIL, sorted by (a) average N_c and (b) average N_p and (c) average N_{cp}.

set	$N_{c,lo}$	$N_{c,hi}$	$N_{c,freq}$	$N_{p,lo}$	$N_{p,hi}$	$N_{p,freq}$	$N_{cp,lo}$	$N_{cp,hi}$	$N_{cp,freq}$
1	—	3.0	7	—	1.8	14	—	1.4	12
2	3.0	3.3	9	1.8	1.9	13	1.4	1.55	110
3	3.3	3.6	103	1.9	2.0	39	1.55	1.7	263
4	3.6	4.9	261	2.0	2.1	84	1.7	1.85	208
5	3.9	4.2	268	2.1	2.2	132	1.85	2.0	121
6	4.2	4.5	102	2.2	2.3	147	2.0	2.15	46
7	4.5	4.8	25	2.3	2.4	163	2.15	2.3	23
8	4.8	—	25	2.4	—	208	2.3	—	17

TABLE S9. Average N_c, N_p, and N_{cp} bin boundaries for each set of MSD data for $n = 5$.

set	$N_{c,lo}$	$N_{c,hi}$	$N_{c,freq}$	$N_{p,lo}$	$N_{p,hi}$	$N_{p,freq}$	$N_{cp,lo}$	$N_{cp,hi}$	$N_{cp,freq}$
1	—	3.0	4	—	1.3	15	—	1.6	53
2	3.0	3.33	31	1.3	1.45	12	1.6	1.75	140
3	3.33	3.66	108	1.45	1.6	16	1.75	1.9	212
4	3.66	4.0	277	1.6	1.75	28	1.9	2.05	165
5	4.0	4.33	204	1.75	1.9	74	2.05	2.2	92
6	4.33	4.66	114	1.9	2.05	212	2.2	2.35	60
7	4.66	5.0	41	2.05	2.2	190	2.35	2.5	38
8	5.0	—	21	2.2	—	253	2.5	—	40

TABLE S10. Average N_c, N_p, and N_{cp} bin boundaries for each set of MSD data for $n = 8$.

the intermittent time autocorrelation functions. Many of the polymeric variants at lower temperatures display poor decay over the lifetime of the simulation. Despite this observation, we fit the stretched exponential function to the curve for every system, extracting a timescale for each one. On the other hand, for the low molecular weight systems, the functions fully decay in as little as 1 ns. Finally, we can see that the smallest timescale that we explored was

set	$N_{c,lo}$	$N_{c,hi}$	$N_{c,freq}$	$N_{p,lo}$	$N_{p,hi}$	$N_{p,freq}$	$N_{cp,lo}$	$N_{cp,hi}$	$N_{cp,freq}$
1	—	3.2	19	—	1.15	33	—	1.7	62
2	3.2	3.33	19	1.15	1.3	17	1.7	1.95	186
3	3.33	3.66	115	1.3	1.45	30	1.95	2.2	283
4	3.66	4.0	281	1.45	1.6	50	2.2	2.45	124
5	4.0	4.33	210	1.6	1.75	79	2.45	2.7	70
6	4.33	4.66	99	1.75	1.9	154	2.7	2.95	27
7	4.66	5.0	41	1.9	2.05	221	2.95	3.2	17
8	5.0	—	20	2.05	—	220	3.2	—	35

TABLE S11. Average N_c, N_p, and N_{cp} bin boundaries for each set of MSD data for $n = 12$.

set	$N_{c,lo}$	$N_{c,hi}$	$N_{c,freq}$	$N_{p,lo}$	$N_{p,hi}$	$N_{p,freq}$	$N_{cp,lo}$	$N_{cp,hi}$	$N_{cp,freq}$
1	—	3.2	33	—	1.15	62	—	1.85	69
2	3.2	3.53	92	1.15	1.3	52	1.85	2.05	118
3	3.53	3.86	190	1.3	1.45	80	2.05	2.25	160
4	3.86	4.2	230	1.45	1.6	74	2.25	2.45	133
5	4.2	4.53	126	1.6	1.75	119	2.45	2.65	106
6	4.53	4.86	72	1.75	1.9	153	2.65	2.85	75
7	4.86	5.2	27	1.9	2.05	167	2.85	3.05	41
8	5.2	—	30	2.05	—	93	3.05	—	98

TABLE S12. Average N_c, N_p, and N_{cp} bin boundaries for each set of MSD data for $n = 16$.

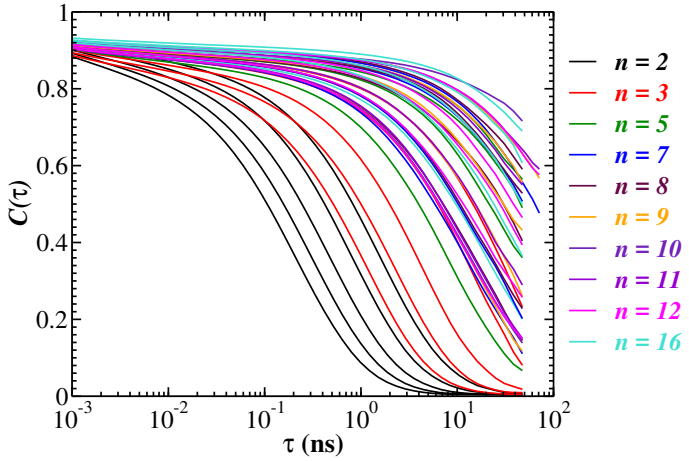

(a)

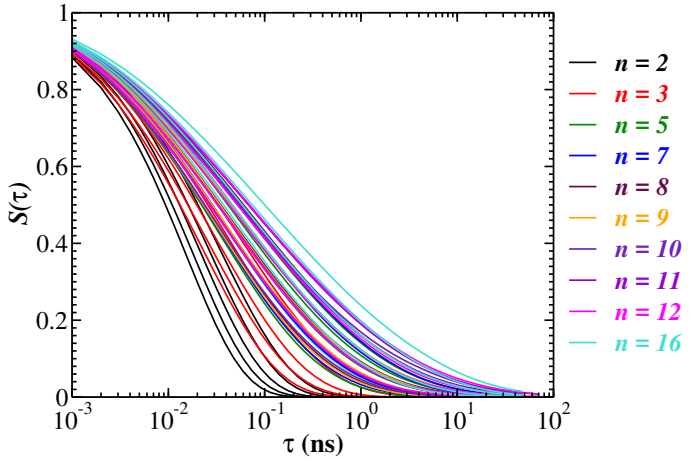

(b)

FIG. S8. (a) $C(\tau)$ and (b) $S(\tau)$ plotted as functions of time.

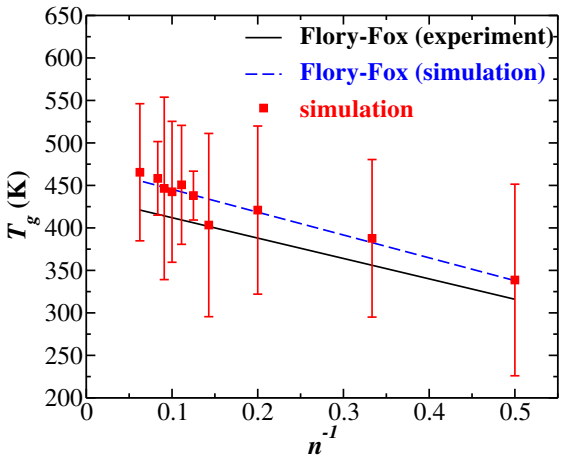

FIG. S9. Plot of glass transition temperature as a function of inverse monomer count n^{-1}, plotted with two Flory-Fox fits (experimental data and simulation data).

1 ps (10^{-3} ns). This is of the order of 0.07-0.12 by visual inspection of Figure 8(a). There is relatively fast and consistent decay within this timescale that is unobserved due to the saving frequency investigated in this analysis. Despite this, we feel confident that our analysis of the qualitative trends extracted by analyzing the timescales for relaxation. This confidence stems from the results presented in Reference 1, which showed the results of analyzing these timescales via autocorrelation functions of varied saving frequency. These results confirmed consistent qualitative trends down to a saving frequency of 0.01 ps, and as high as 100 ps. Since these tests were conducted on the same polyIL as the one investigated in the present article, we refrained from pursuing further justification of the assumption that this saving frequency is appropriate to extract the timescales of physical behaviors of interest. It is important to note that this behavior extends to the analysis of ion hopping, including the frequency of intra- and intermolecular hopping events presented in the main article. These measures were also explored in Reference 1 for qualitative consistency with varying saving frequency, with positive results.

D. Glass transition temperatures

As we explained in the main article, we made the choice to preserve the glass-transition temperatures (T_g) as a value of experimental origin. Figure S9 presents the T_g values as

calculated by simulation. The method used to capture these glass transition temperatures by simulation involves anlyzing the slope of the density versus temperature curve over the appropriate range of transistion. Despite this being a widely used and accepted method for extracting this transition temperature in such applications, it is prone to high errors, as depicted by our representation of the error bars in the same figure. The curve generated by the Flory-Fox equation, fit to experimental values of T_g, is shown in the same figure. This curve represents the set of T_g that we ultimately used to express our findings in Figures 2(b) and 4 of the main article. The dotted line represents the Flory-Fix fit to the simulation data, and shows a small deviation in slope, but nonetheless, bears a close resemblance to the experimental Flory-Fox fitting curve, lending credibility to our choice.

III. EXPLORING DENSITY AND EQUILIBRATION OF THE SYSTEM

A. Verifying the stability of the systems under investigation

Our methods for initialization and equilibration are covered in detail by the main paper. Here, we present evidence that suggests that our systems have found stable, equilibrium operating points. Figure S10 shows both the potential enegy U and the total energy E, as function of the simulation time, for the systems under investigation. The consistency of these values across the length of the production simulation indicates that there is stability in these system configurations. Figure S11 offers further proof of this stability, showing that the density is also constant across the same interval of simulation time. Together, these measures are convincing in justifying the conclusions within the present article as representative for polyIL electrolytes at equilibrium.

B. Density as a function of linker size

We present the density ρ as a function of n in Figure S12, showing that density behaves similarly to the diffusivity (Figure 2(a)) and ion-association relaxation times (Figures 3 and 11) discussed in the main paper. Therefore, it is impossible to separate these measures given

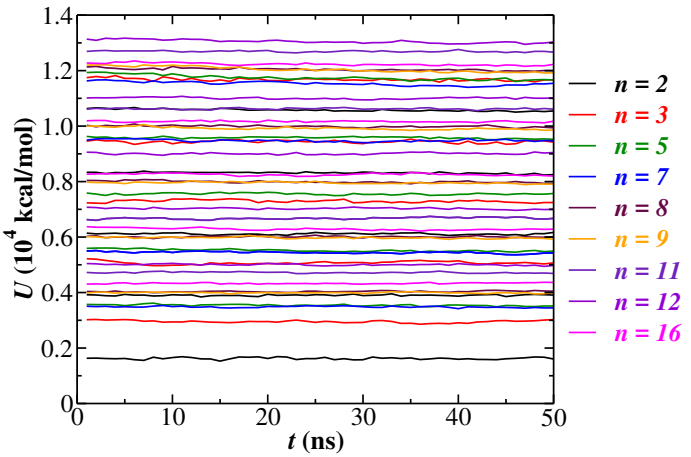

(a)

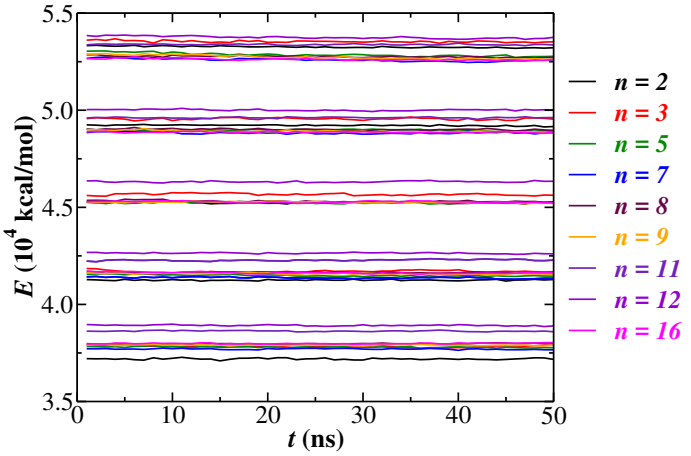

(b)

FIG. S10. Temporal plot of (a) potential energy U and (b) total energy E over the full MD simulation length. Recorded values are averages over every 0.5 ns.

the data presented in this work.

REFERENCES

[1]S. Mogurampelly, J. Keith, and V. Ganesan, Journal of the American Chemical Society **139**, 9511 (2017).

[2]W. L. Jorgensen, D. S. Maxwell, and J. Tirado-Rives, J. Am. Chem. Soc. **118**, 11225 (1996).

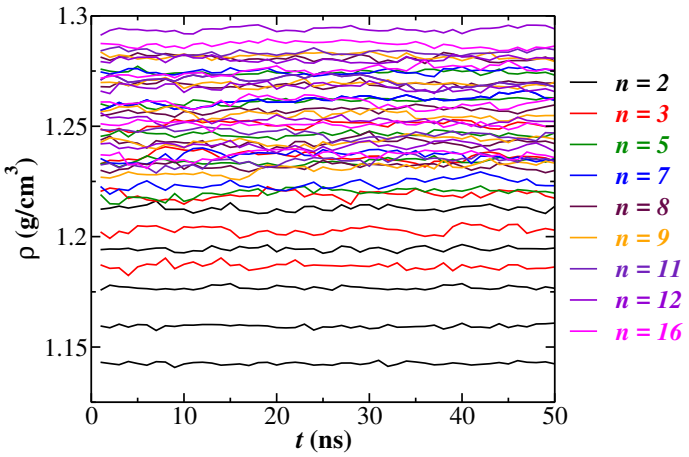

FIG. S11. Temporal plot of density ρ over the full MD simulation length. Recorded values are averages over every 0.5 ns.

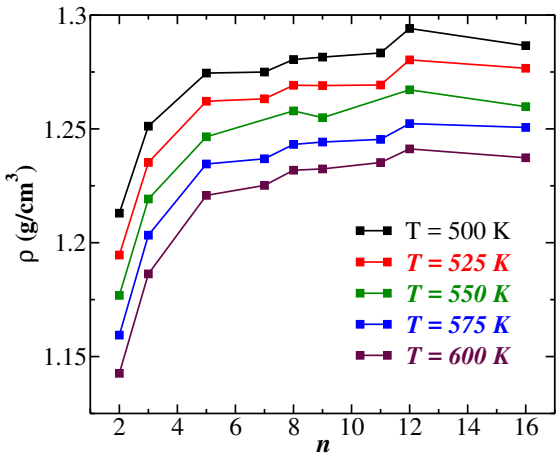

FIG. S12. Plot of density ρ versus the number of monomers n.

[3]S. V. Sambasivarao and O. Acevedo, Journal of Chemical Theory and Computation **5**, 1038 (2009).

[4]B. L. Bhargava and S. Balasubramanian, Journal of Chemical Physics **127**, 114510 (2007).